# The Design of a Chain of Spherical Stephenson Mechanisms for a Gearless Robotic Pitch-Roll Wrist

**S. Hernandez**

**S. Bai**
e-mail: mspbai@cim.mcgill.ca

**J. Angeles**
e-mail: angeles@cim.mcgill.ca

Department of Mechanical Engineering
& Centre for Intelligent Machines,
McGill University,
Montreal, QC H3A 2A7 Canada

*Although bevel-gear robotic wrists are widely used in industrial manipulators due to their simple kinematics and low manufacturing cost, their gear trains function under rolling and sliding, the latter bringing about noise and vibration. Sliding is inherent to the straight teeth of the bevel gears of these trains. Moreover, unavoidable backlash introduces unmodeled dynamics, which mars robot performance. To alleviate these drawbacks, a gearless pitch-roll wrist is currently under development for low backlash and high stiffness. The wrist consists of spherical cam-rollers and spherical Stephenson linkages, besides two roller-carrying disks that drive a combination of cams and Stephenson mechanisms, the whole system rotating as a differential mechanism. The paper focuses on the design of the chain of spherical Stephenson mechanisms. The problem of the dimensional synthesis is addressed, and interference avoidance is discussed. An embodiment of the concept is also included.* [DOI: 10.1115/1.2167653]

*Keywords: spherical Stephenson mechanism, dimensional synthesis, nonlinear least-square optimization, pitch-roll wrists*

## 1 Introduction

Robotic wrists are commonly used in manipulators for applications that require a large dexterous workspace [1–5]. As a robotic wrist is to be attached to a moving arm, it is desirable to design such wrists with light weight, low backlash, and high stiffness. Some industrial wrists, like the Cincinnati Milacron $T^3$ and the Bendix wrist, were designed with bevel-gear trains in a differential array [4]. For bevel-gear wrists, the kinematics is simple and the manufacturing cost is relatively low if gears with straight teeth are used. However, such gear trains function under rolling and sliding, the latter bringing about noise and vibration. To alleviate these drawbacks, spiral teeth can be used [6], but at such a cost that, to our knowledge, no robot manufacturer has adopted spiral bevel gears for wrist design. Moreover, unavoidable backlash introduces unmodeled dynamics, which mars robot performance. Attempts have been made to design wrists with different approaches for a better performance: Wiitala and Stanisic proposed a wrist design based on a symmetrically actuated spherical eight-bar linkage [7], which can eliminate the singularity within its hemispherical workspace; a three-degree-of-freedom (three-dof) parallel spherical wrist, called "Agile Wrist," was developed for high accuracy and high precision [8], derived from the isotropic design of Gosselin's "Agile Eye" [9]; other wrist designs can also be found in [1,5].

A pitch-roll robotic wrist based on spherical cam-rollers, which bears features of high stiffness and low backlash [10–12], is being developed at McGill University with the aim of replacing its bevel-gear counterparts in robotic manipulators [10]. As shown in Fig. 1, the wrist adopts a two-layer structure. The outer layer consists of two roller-carrying disks (RCDs), each driven by one motor. The inner layer is a three-cam subassembly driven by RCDs that rotate as the sun gears of a differential mechanism. These three cam-shaft subassemblies are used in order to balance the mechanism. Each subassembly consists of a pair of conjugate spherical cams, which guarantees positive action of the rollers onto the cams. However, coaxial conjugate cams are difficult to machine out of one single block, as required to meet our tight tolerance requirements. To solve this problem, a new design is proposed with spherical Stephenson mechanisms. These mechanisms, combined with cams, are to replace the inner layer of the pitch-roll wrist. In the alternative design, the conjugate cams are rigidly mounted on two different shafts, the rotations of the cams being transmitted to the gripper by an array of spherical Stephenson mechanisms. In this way, the manufacturing cost is greatly reduced, while the assembly accuracy is expected to be enhanced.

The design of spherical Stephenson mechanisms (SSMs) for a gearless pitch-roll wrist is discussed here. The problem of the dimensional synthesis is addressed and interference-avoidance is given due consideration. The paper is organized in five sections: The kinematics of the SSM is studied in Sec. 2, where the associated input-output (IO) equations are derived. In Sec. 3, a method of dimensional synthesis is developed by formulating the synthesis problem as the least-square approximation of an unconstrained nonlinear system of algebraic equations; its least-square approximation yields the optimum linkage sought. The design of the SSM is described in Sec. 4, where design problems such as link shape, link dimensioning, the SSM layout, and interference-avoidance are discussed. The work concludes in Sec. 5.

## 2 The Kinematics of the SSM

The classical Stephenson mechanism is a six-bar planar linkage that was originally designed to control the motion of a steam engine [13]. Its four binary and two ternary links form two loops in its kinematic chain. Depending on the link that serves as the base, Stephenson mechanisms are classified into three types [13].

Stephenson mechanisms can remarkably extend the motion capability of four-bar linkages. For example, a Stephenson mechanism can meet up to 11 poses of one of its floating links, as opposed to the five poses of four-bar linkages [14], and nine of the Watt linkage [15]. On the other hand, the analysis and synthesis of Stephenson mechanisms are much more complex. Due to the pres-

Contributed by the Mechanisms and Robotics Committee of ASME for publication in the JOURNAL OF MECHANICAL DESIGN. Manuscript received April 26, 2005; final manuscript received June 6, 2005. Review conducted by Madhu Raghavan.

  

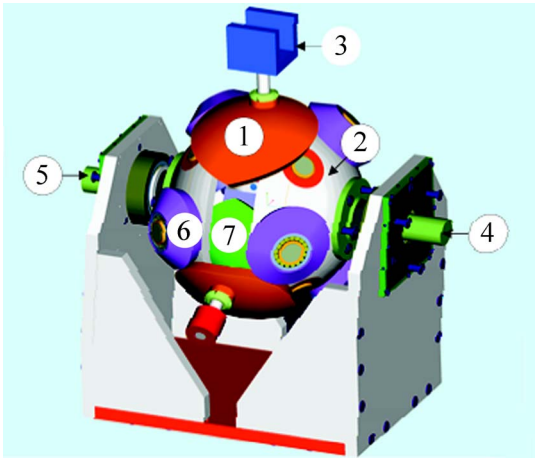


**Fig. 1 Gearless pitch-roll wrist based on cam-rollers: (1) outer cam; (2) roller-carrying disk; (3) gripper; (4) and (5) input shafts connected to the two motors; (6) roller; (7) inner cam**

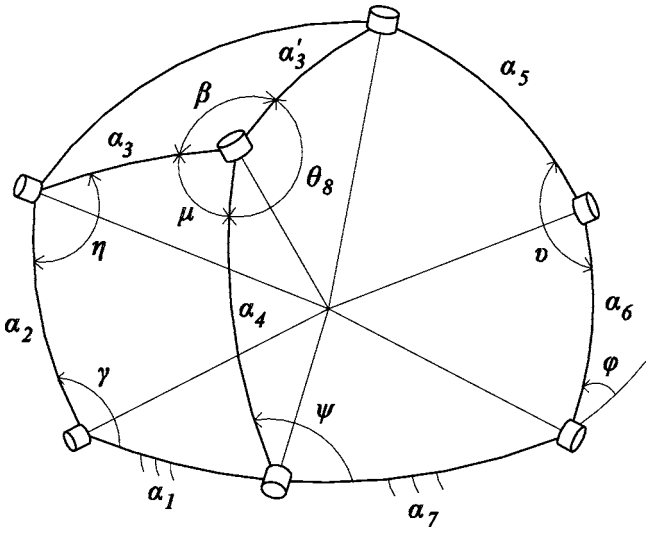


**Fig. 2 A spherical Stephenson mechanism**

ence of two independent loops in the kinematic chain of Stephenson mechanisms, a closed form of its input-output equation is difficult to derive. Zanganeh and Angeles [16] derived a symbolic input-output equation of planar Stephenson mechanisms. Other works that are relevant to the kinematic analysis and synthesis of planar Stephenson mechanisms can be cited [17–20]. Of these works, Dhingra et al. [18] investigated the path-generation problem for six-bar linkages using homotopy, while Sakamoto et al. [20] studied the interference problem of six-bar mechanisms.

Spherical Stephenson mechanisms are six-bar spherical linkages analogous to their planar counterparts. The joint axes of a spherical Stephenson mechanism intersect at one point, all links moving on spherical surfaces centered at this point. Although numerous publications dealing with four- and five-bar spherical mechanisms are available [21–26], the problem of analysis and synthesis of spherical Stephenson mechanisms is yet to be reported.

The synthesis method we propose here is based on the input-output equation of the spherical Stephenson mechanism, which is derived from the four- and five-bar loops of the mechanism. Although the derivation of the former is well documented, we recall it here for completeness, and report on the derivation of the latter. The novel unified approach proposed by Wampler [27], which is generally applicable to multiloop spherical linkages, was used to derive the two-loop equations.

**2.1 SSM Modeling.** The kinematic chain of a spherical Stephenson mechanism is illustrated in Fig. 2. This mechanism comprises six links connected by seven revolute joints; the linkage forms two loops, the four-bar loop (left-hand side) and the five-bar loop (right-hand side), coupled by means of a ternary link. For the sake of conciseness, we refer to the various binary links by the labels of the arcs that define every such link.

**2.2 IO Equations of the Two Loops.** To illustrate the application of Wampler's method, which eases the derivation of the input-output equation of the five-link loop, we derive first that of the four-link loop. To this end, we proceed by defining the coordinate frames at each joint, as shown in Fig. 3. We define first a set of coordinate axes at each joint aligning the $z$-axis with the axis of rotation of the joint. The $x$ and $y$ axes can be given any orientation normal to $z$, so as to form a right-handed orthogonal coordinate system. The assumption that the links are rigid implies that the relative orientation between any two coordinate systems fixed to the same link is constant. Such rotations are called "side rotations" of the link. The $x$-axis is taken as the axis of rotation. In traversing a spherical-mechanism loop, two types of rotations are found: *joint rotations*, which are variable, and *side rotations*, which are constant.

To end up with a loop equation in trigonometric form as a function only of the input and output angles $\gamma$ and $\psi$, respectively, we chose the loop equation so as to eliminate the two other joint angles. Hence, the loop equation is taken as

$$\mathbf{Z}_4\mathbf{S}_4\mathbf{Z}_1\mathbf{S}_1\mathbf{Z}_2\mathbf{S}_2\mathbf{Z}_3\mathbf{S}_3 = \mathbf{1} \tag{1}$$

where $\mathbf{1}$ is the $3\times3$ identity matrix, while $\mathbf{Z}_1=\mathbf{R}_z(\psi)$, $\mathbf{Z}_2=\mathbf{R}_z(\pi-\gamma)$, $\mathbf{Z}_3=\mathbf{R}_z(\theta_3)$, and $\mathbf{Z}_4=\mathbf{R}_z(\theta_4)$, with

$$\mathbf{R}_z(\cdot) = \begin{bmatrix} \cos(\cdot) & -\sin(\cdot) & 0 \\ \sin(\cdot) & \cos(\cdot) & 0 \\ 0 & 0 & 1 \end{bmatrix}$$

Notice that Wampler's method uses exterior angles at each vertex, instead of interior angles, matrix $\mathbf{Z}_2$ being a function of the interior angle $\gamma$. Moreover, $\mathbf{S}_1=\mathbf{R}_x(\alpha_1)$, $\mathbf{S}_2=\mathbf{R}_x(\alpha_2)$, $\mathbf{S}_3=\mathbf{R}_z(\alpha_3)$, and $\mathbf{S}_4=\mathbf{R}_x(\alpha_4)$, with

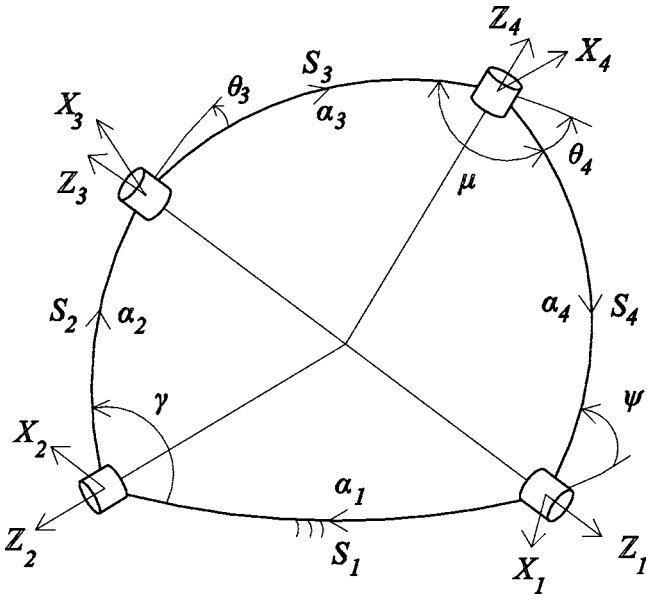


**Fig. 3 The four-bar loop**

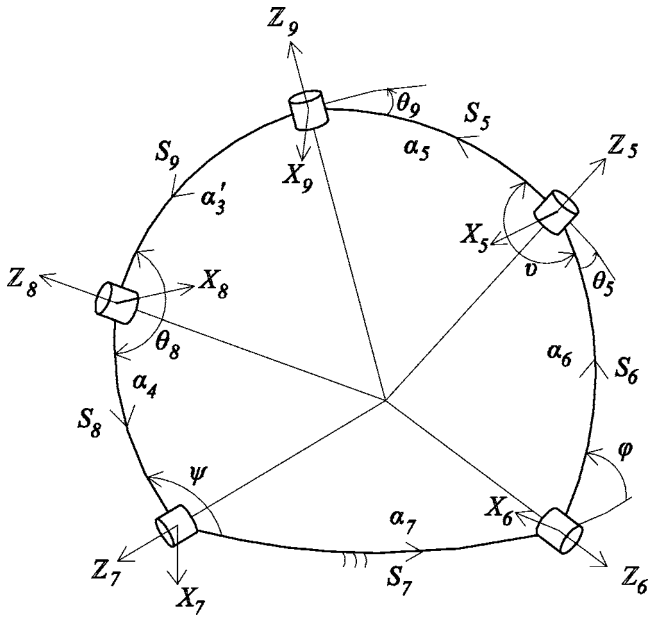


**Fig. 4 The five-bar loop**

$$\mathbf{R}_x(\cdot)=\begin{bmatrix}1 & 0 & 0\\ 0 & \cos(\cdot) & -\sin(\cdot)\\ 0 & \sin(\cdot) & \cos(\cdot)\end{bmatrix}$$

We eliminate the joint matrices $\mathbf{Z}_3$ and $\mathbf{Z}_4$ from Eq. (1) to have the loop equation in terms of the input and output angles alone. We do this by means of the relation

$$\mathbf{z}_4^T\mathbf{Z}_4\mathbf{S}_4\mathbf{Z}_1\mathbf{S}_1\mathbf{Z}_2\mathbf{S}_2\mathbf{Z}_3\mathbf{z}_3=\mathbf{z}_4^T\mathbf{S}_3^T\mathbf{z}_3 \tag{2}$$

where $\mathbf{z}_i=[0\ 0\ 1]^T$; hence, the loop equation is obtained as

$$\mathbf{z}^T\mathbf{S}_4\mathbf{Z}_1\mathbf{S}_1\mathbf{Z}_2\mathbf{S}_2\mathbf{z}=\mathbf{z}_4^T\mathbf{S}_3^T\mathbf{z}_3 \tag{3}$$

with $\mathbf{z}=[0\ 0\ 1]^T$.

Equation (3) yields the loop equation of the four-bar loop in trigonometric form, namely,

$$\begin{aligned}f(\gamma,\psi,\boldsymbol{\alpha})=&\,\mathrm{s}\alpha_2\mathrm{s}\alpha_4\mathrm{s}\gamma\mathrm{s}\psi+\mathrm{c}\alpha_1\mathrm{s}\alpha_2\mathrm{s}\alpha_4\mathrm{c}\gamma\mathrm{c}\psi+\mathrm{s}\alpha_1\mathrm{s}\alpha_2\mathrm{c}\alpha_4\mathrm{c}\theta\\&-\mathrm{s}\alpha_1\mathrm{c}\alpha_2\mathrm{s}\alpha_4\mathrm{c}\psi+\mathrm{c}\alpha_1\mathrm{c}\alpha_2\mathrm{c}\alpha_4-\mathrm{c}\alpha_3\\=&\,0\end{aligned} \tag{4}$$

in which $s$ and $c$ represent the sine and cosine trigonometric functions, respectively, while

$$\boldsymbol{\alpha}\equiv[\alpha_1\ \alpha_2\ \alpha_3\ \alpha_4]^T \tag{5}$$

Equation (4) is the input-output equation of the four-bar linkage.

Figure 4 shows the coordinate axes at each joint of the five-bar loop. For this loop we also want to end up with a loop equation in trigonometric form that contains the input and output angles $\psi$ and $\phi$ only, and no other joint angle of the loop. From Fig. 4 we can see that now we have five joints, from which we can eliminate only two by their respective joint rotations, so that the trigonometric form of the loop equation, besides the input and output angles, will contain an extra joint angle. Hence, we chose the loop equation in a form that allows us to eliminate the joint rotations $\mathbf{Z}_5$ and $\mathbf{Z}_9$, and keep the joint rotations $\mathbf{Z}_6$ and $\mathbf{Z}_7$ that represent the output and input angles as well as the joint rotation $\mathbf{Z}_8$; the latter is common to both the four-bar and the five-bar loops of the spherical Stephenson mechanism.

Thus, the loop-equation that we choose is

$$\mathbf{Z}_9\mathbf{S}_9\mathbf{Z}_8\mathbf{S}_8\mathbf{Z}_7\mathbf{S}_7\mathbf{Z}_6\mathbf{S}_6\mathbf{Z}_5\mathbf{S}_5=\mathbf{1} \tag{6}$$

where $\mathbf{1}$ is the $3\times3$ identity matrix, while $\mathbf{Z}_5=\mathbf{R}_z(\theta_5)$, $\mathbf{Z}_6=\mathbf{R}_z(\phi)$, $\mathbf{Z}_7=\mathbf{R}_z(\pi-\psi)$, $\mathbf{Z}_8=\mathbf{R}_z(\pi-\theta_8)$, and $\mathbf{Z}_9=\mathbf{R}_z(\theta_9)$.

Matrices $\mathbf{Z}_7$ and $\mathbf{Z}_8$ are formulated to involve the internal angles $\psi$ and $\theta_8$, respectively. Moreover, $\mathbf{S}_5=\mathbf{R}_x(\alpha_5)$, $\mathbf{S}_6=\mathbf{R}_x(\alpha_6)$, $\mathbf{S}_7=\mathbf{R}_z(\alpha_7)$, $\mathbf{S}_8=\mathbf{R}_x(\alpha_4)$, and $\mathbf{S}_9=\mathbf{R}_x(\alpha_3')$.

In order to eliminate the joint rotations $\mathbf{Z}_5$ and $\mathbf{Z}_9$ we resort to the relation

$$\mathbf{z}_9^T\mathbf{Z}_9\mathbf{S}_9\mathbf{Z}_8\mathbf{S}_8\mathbf{Z}_7\mathbf{S}_7\mathbf{Z}_6\mathbf{S}_6\mathbf{Z}_5\mathbf{z}_5=\mathbf{z}_9^T\mathbf{S}_5^T\mathbf{z}_5 \tag{7}$$

which simplifies to

$$\mathbf{z}^T\mathbf{S}_9\mathbf{Z}_8\mathbf{S}_8\mathbf{Z}_7\mathbf{S}_7\mathbf{Z}_6\mathbf{S}_6\mathbf{z}=\mathbf{z}_9^T\mathbf{S}_5^T\mathbf{z}_5 \tag{8}$$

Furthermore, to eliminate the undesired angle $\theta_8$, we express both $\cos\theta_8$ and $\sin\theta_8$ using what is known as the tan-half identities, namely,

$$\cos\theta_8=\frac{1-t_8^2}{1+t_8^2}\quad \sin\theta_8=\frac{2t_8}{1+t_8^2}\quad t_8=\tan(\theta_8/2) \tag{9}$$

With these substitutions, we define $\bar{\mathbf{Z}}_8$ as

$$\bar{\mathbf{Z}}_8=\begin{bmatrix}-(1-t_8^2) & -2t_8 & 0\\ 2t_8 & -(1-t_8^2) & 0\\ 0 & 0 & (1+t_8^2)\end{bmatrix} \tag{10}$$

Thus, Eq. (8) becomes

$$\mathbf{z}^T\mathbf{S}_9\bar{\mathbf{Z}}_8\mathbf{S}_8\mathbf{Z}_7\mathbf{S}_7\mathbf{Z}_6\mathbf{S}_6\mathbf{z}=\mathbf{z}_9^T\mathbf{S}_5^T\mathbf{z}_5(1+t_8^2) \tag{11}$$

Equation (11) yields the five-bar loop equation in trigonometric form, namely,

$$g(t_8;\tilde{\boldsymbol{\alpha}})=At_8^2+Bt_8+C=0 \tag{12}$$

where

$$\tilde{\boldsymbol{\alpha}}\equiv[\alpha_3'\ \alpha_4\ \alpha_5\ \alpha_6\ \alpha_7]^T \tag{13a}$$

$$\begin{aligned}A(\psi,\phi;\tilde{\boldsymbol{\alpha}})=&-\mathrm{s}\alpha_6\mathrm{s}\phi\mathrm{s}\psi\mathrm{s}\alpha_3'\mathrm{c}\alpha_4-\mathrm{s}\alpha_6\mathrm{c}\phi\mathrm{c}\alpha_7\mathrm{c}\psi\mathrm{s}\alpha_3'\mathrm{c}\alpha_4\\&+\mathrm{s}\alpha_6\mathrm{s}\phi\mathrm{s}\psi\mathrm{c}\alpha_3'\mathrm{s}\alpha_4+\mathrm{s}\alpha_6\mathrm{c}\phi\mathrm{c}\alpha_7\mathrm{c}\psi\mathrm{c}\alpha_3'\mathrm{s}\alpha_4\\&-\mathrm{s}\alpha_6\mathrm{c}\phi\mathrm{s}\alpha_7\mathrm{c}\alpha_3'\mathrm{c}\alpha_4-\mathrm{s}\alpha_6\mathrm{c}\phi\mathrm{s}\alpha_7\mathrm{s}\alpha_3'\mathrm{s}\alpha_4\\&+\mathrm{c}\alpha_6\mathrm{s}\alpha_7\mathrm{c}\psi\mathrm{c}\alpha_3'\mathrm{s}\alpha_4+\mathrm{c}\alpha_6\mathrm{c}\alpha_7\mathrm{s}\alpha_3'\mathrm{s}\alpha_4+\mathrm{c}\alpha_6\mathrm{c}\alpha_7\mathrm{c}\alpha_3'\mathrm{c}\alpha_4\\&-\mathrm{c}\alpha_6\mathrm{s}\alpha_7\mathrm{c}\psi\mathrm{s}\alpha_3'\mathrm{c}\alpha_4-\mathrm{c}\alpha_5\end{aligned} \tag{13b}$$

$$B(\psi,\phi;\tilde{\boldsymbol{\alpha}})=2\mathrm{s}\alpha_6\mathrm{c}\phi\mathrm{c}\alpha_7\mathrm{s}\alpha_3'\mathrm{s}\psi-2\mathrm{s}\alpha_6\mathrm{s}\phi\mathrm{s}\alpha_3'\mathrm{c}\psi+2\mathrm{c}\alpha_6\mathrm{s}\alpha_7\mathrm{s}\alpha_3'\mathrm{s}\psi \tag{13c}$$

$$\begin{aligned}C(\psi,\phi;\tilde{\boldsymbol{\alpha}})=&-\mathrm{s}\alpha_6\mathrm{c}\phi\mathrm{s}\alpha_7\mathrm{c}\alpha_3'\mathrm{c}\alpha_4+\mathrm{s}\alpha_6\mathrm{c}\phi\mathrm{c}\alpha_7\mathrm{c}\psi\mathrm{c}\alpha_3'\mathrm{s}\alpha_4\\&+\mathrm{c}\alpha_6\mathrm{s}\alpha_7\mathrm{c}\psi\mathrm{s}\alpha_3'\mathrm{c}\alpha_4+\mathrm{s}\alpha_6\mathrm{c}\phi\mathrm{c}\alpha_7\mathrm{c}\psi\mathrm{s}\alpha_3'\mathrm{c}\alpha_4\\&+\mathrm{s}\alpha_6\mathrm{s}\phi\mathrm{s}\psi\mathrm{c}\alpha_3'\mathrm{s}\alpha_4+\mathrm{s}\alpha_6\mathrm{c}\phi\mathrm{s}\alpha_7\mathrm{s}\alpha_3'\mathrm{s}\alpha_4\\&+\mathrm{s}\alpha_6\mathrm{s}\phi\mathrm{s}\psi\mathrm{s}\alpha_3'\mathrm{c}\alpha_4+\mathrm{c}\alpha_6\mathrm{c}\alpha_7\mathrm{c}\alpha_3'\mathrm{c}\alpha_4-\mathrm{c}\alpha_6\mathrm{c}\alpha_7\mathrm{s}\alpha_3'\mathrm{s}\alpha_4\end{aligned} \tag{13d}$$

**2.3 The IO Equation of the SSM.** By combining the equations of the two loops and eliminating the common angle $\theta_8$, the input-output equation of the SSM can be obtained.

In order to couple the five-bar with the four-bar loop, we need to make Eq. (4) a function of $\theta_8$. An equation for the angles $\mu$ and $\gamma$ is further derived from the geometry of the linkage,

$$\mathrm{c}\gamma=\frac{\mathrm{s}\alpha_3\mathrm{s}\alpha_4\mathrm{c}\mu+\mathrm{c}\alpha_3\mathrm{c}\alpha_4-\mathrm{c}\alpha_1\mathrm{c}\alpha_2}{\mathrm{s}\alpha_1\mathrm{s}\alpha_2} \tag{14}$$

From Fig. 2 we notice that $\mu=2\pi-(\beta+\theta_8)$, which, when substituted into Eq. (14), leads to

$$c\gamma = \frac{s\alpha_3 s\alpha_4 c(\beta+\theta_8) + c\alpha_3 c\alpha_4 - c\alpha_1 c\alpha_2}{s\alpha_1 s\alpha_2} \tag{15}$$

The above expression is now substituted into Eq. (4). Expressing $\cos\theta_8$ and $\sin\theta_8$ using the tan-half identities of Eq. (9), the four-bar loop equation becomes

$$f(t_8;\boldsymbol{\alpha},\beta) = Dt_8^2 + Et_8 + F = 0 \tag{16}$$

where

$$\begin{aligned} D(\psi,\gamma;\boldsymbol{\alpha},\beta) = {} & c\psi c\alpha_1 s\alpha_3 c\beta c\alpha_4^2 + s\alpha_4 c\psi c\alpha_1 c\alpha_3 c\alpha_4 \\ & - c\alpha_4 s\alpha_1 s\alpha_3 s\alpha_4 c\beta + c\alpha_4^2 s\alpha_1 c\alpha_3 + s\alpha_2 s\alpha_4 s\psi s\gamma s\alpha_1 \\ & - c\psi c\alpha_1 s\alpha_3 c\beta - c\alpha_2 s\alpha_4 c\psi - c\alpha_3 s\alpha_1 \end{aligned} \tag{17a}$$

$$\begin{aligned} E(\psi,\gamma,\boldsymbol{\alpha},\beta) = {} & -2c\psi c\alpha_1 s\alpha_3 s\beta + 2c\psi c\alpha_1 s\alpha_3 s\beta c\alpha_4^2 \\ & - 2c\alpha_4 s\alpha_1 s\alpha_3 s\alpha_4 s\beta \end{aligned} \tag{17b}$$

$$\begin{aligned} F(\psi,\gamma;\boldsymbol{\alpha},\beta) = {} & c\psi c\alpha_1 s\alpha_3 c\beta - c\psi c\alpha_1 s\alpha_3 c\beta c\alpha_4^2 - c\alpha_2 s\alpha_4 c\psi \\ & + s\alpha_4 c\psi c\alpha_1 c\alpha_3 c\alpha_4 + s\alpha_2 s\alpha_4 s\psi s\gamma s\alpha_1 + c\alpha_4^2 s\alpha_1 c\alpha_3 \\ & - c\alpha_3 s\alpha_1 + c\alpha_4 s\alpha_1 s\alpha_3 s\alpha_4 c\beta \end{aligned} \tag{17c}$$

To obtain the SSM input-output equation, we need to eliminate $t_8$ from Eqs. (12) and (16). This can be done via *dialytic elimination* [28], as described below.

We start by recalling Eqs. (12) and (16)

$$g(t_8;\tilde{\boldsymbol{\alpha}}) = At_8^2 + Bt_8 + C = 0 \tag{18a}$$

$$f(t_8;\boldsymbol{\alpha},\beta) = Dt_8^2 + Et_8 + F = 0 \tag{18b}$$

Further, we derive two additional equations from Eqs. (18*a*) and (18*b*) by multiplying the two sides of each of these equations by $t_8$, thereby obtaining a total of four polynomial equations in $t_8$, namely,

$$At_8^3 + Bt_8^2 + Ct_8 = 0 \tag{19a}$$

$$Dt_8^3 + Et_8^2 + Ft_8 = 0 \tag{19b}$$

$$At_8^2 + Bt_8 + C = 0 \tag{19c}$$

$$Dt_8^2 + Et_8 + F = 0 \tag{19d}$$

Now, we write the above four equations in *linear homogeneous form*,

$$\mathbf{M}\mathbf{t}_8 = \mathbf{0} \tag{20}$$

where the $4\times4$ matrix $\mathbf{M}$ and the four-dimensional vector $\mathbf{t}_8$ are defined as

$$\mathbf{M} = \begin{bmatrix} A & B & C & 0 \\ D & E & F & 0 \\ 0 & A & B & C \\ 0 & D & E & F \end{bmatrix} \quad \mathbf{t}_8 = \begin{bmatrix} t_8^3 \\ t_8^2 \\ t_8 \\ 1 \end{bmatrix} \tag{21}$$

Since $\mathbf{t}_8$ cannot vanish, Eq. (20) must admit a nontrivial solution, and hence, $\mathbf{M}$ must be singular, i.e.,

$$q(\psi,\gamma,\phi;\hat{\boldsymbol{\alpha}},\beta) = \det(\mathbf{M}) = 0 \tag{22}$$

with

$$\hat{\boldsymbol{\alpha}} \equiv [\alpha_1\ \alpha_2\ \alpha_3\ \alpha_3'\ \alpha_4\ \alpha_5\ \alpha_6\ \alpha_7]^T \tag{23}$$

$$\begin{aligned} \det(\mathbf{M}) = {} & AEBF - ACE^2 - A^2F^2 + 2ADFC - DB^2F + DBCE \\ & - D^2C^2 \end{aligned} \tag{24}$$

Equation (22) expresses the relationship among all link dimensions and the input-output angles, $\gamma$, $\psi$, and $\phi$. This equation can be used for either the analysis of the SSM with a given set of linkage dimensions or its dimensional synthesis, as outlined in Sec. 3.

## 3 Dimensional Synthesis

To synthesize the SSM, we introduce first the nine-dimensional design vector

$$\mathbf{y} = [\alpha_1\ \alpha_2\ \alpha_3\ \alpha_3'\ \alpha_4\ \alpha_5\ \alpha_6\ \alpha_7\ \beta]^T \tag{25}$$

If the desired motion of a SSM is specified by $m$ input-output triads $\{\psi_i,\phi_i,\gamma_i\}_{i=1}^m$, with $m>9$, the dimension of $\mathbf{y}$, then a problem of *approximate synthesis* is formulated. After substituting $\{\psi_i,\phi_i,\gamma_i\}_{i=1}^m$ into Eq. (22), we obtain

$$q_i = q(\mathbf{d}_i;\mathbf{y}) = \det(\mathbf{M}_i) = 0 \tag{26}$$

where $\mathbf{d}_i=[\psi_i,\phi_i,\gamma_i]^T$, for $i=1,\ldots,m$ and $\mathbf{M}_i$ is a function of the $i$th input-output triad.

Moreover, if we adjoin the reference angles $\psi_0$, $\phi_0$, and $\gamma_0$ of the SSM to the list of design variables, then we end up with a 12-dimensional design vector $\bar{\mathbf{y}}$

$$\bar{\mathbf{y}} = [\alpha_1\ \alpha_2\ \alpha_3\ \alpha_3'\ \alpha_4\ \alpha_5\ \alpha_6\ \alpha_7\ \beta\ \psi_0\ \phi_0\ \gamma_0]^T \tag{27}$$

Further, let us rewrite the input and output angles in an incremental form, namely,

$$\psi_i = \psi_0 + \Delta\psi_i \quad \phi_i = \phi_0 + \Delta\phi_i \quad \gamma_i = \gamma_0 + \Delta\gamma_i \tag{28}$$

Eq. (22) thus taking the form

$$q_i = q(\Delta\mathbf{d}_i;\bar{\mathbf{y}}) = 0, \quad i = 1,\ldots,m \tag{29}$$

where $\Delta\mathbf{d}_i=[\Delta\psi_i,\Delta\phi_i,\Delta\gamma_i]^T$.

Let

$$x_i = \tan(\alpha_i/2) \quad i = 1,\ldots,7 \tag{30a}$$

$$x_8 = \tan(\alpha_3'/2) \tag{30b}$$

$$x_9 = \tan(\beta/2) \tag{30c}$$

$$x_{10} = \tan(\psi_0/2) \tag{30d}$$

$$x_{11} = \tan(\gamma_0/2) \tag{30e}$$

$$x_{12} = \tan(\phi_0/2) \tag{30f}$$

and

$$\cos\alpha_i = \frac{1-x_i^2}{1+x_i^2} \tag{31a}$$

$$\sin\alpha_i = \frac{2x_i}{1+x_i^2} \quad i = 1,\ldots,7 \tag{31b}$$

and similar relations for $x_8,\ldots,x_{12}$. We thereby define a system of $m$ nonlinear equations in 12 unknowns, namely,

$$\mathbf{q}(\mathbf{x}) = \mathbf{0}$$

where $\mathbf{q}=[q_1,\ldots,q_m]^T$ and $\mathbf{x}=[x_1,\ldots,x_{12}]^T$. For $m>12$, this is an overdetermined system of nonlinear equations whose least-square approximation yields the optimum linkage sought [29]. The associated unconstrained nonlinear least-square problem is thus

$$\min_{\mathbf{x}} \frac{1}{2}\mathbf{q}^T\mathbf{W}\mathbf{q} \tag{32}$$

where $\mathbf{W}$ is an $m\times m$ positive-definite weighting matrix. When all the $m$ components of vector $\mathbf{q}$ are considered with the same weight, the weighting matrix $\mathbf{W}$ can be defined as a multiple of the $m\times m$ identity matrix $\mathbf{1}$, namely,

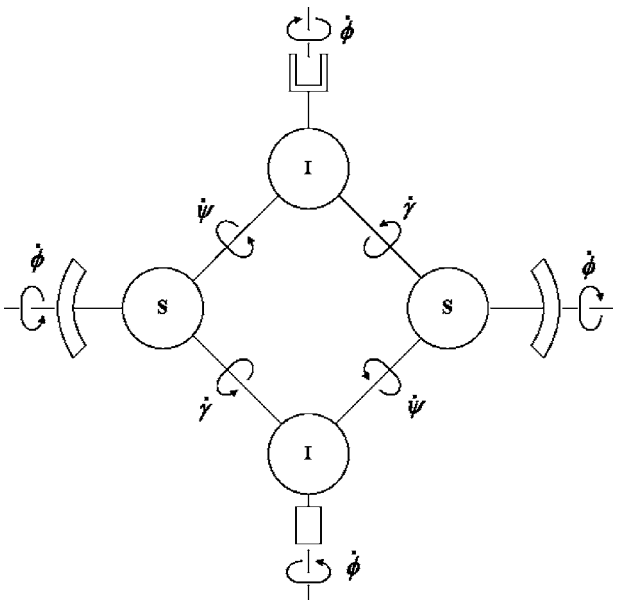


**Fig. 5 Arrangement of Stephenson mechanisms for rotation reversal**

$$\mathbf{W} = \frac{1}{m}\mathbf{1} \tag{33}$$

and the objective function of Eq. (32) becomes one-half the square of the rms value of the $m$ components of $\mathbf{q}$.

## 4 The SSM Design

**4.1 Layout of the SSM.** As mentioned in Sec. 1, four SSMs are used in the pitch-roll wrist to couple the cam rotation to that of the gripper. To this end, the four SSMs are grouped into two pairs: one pair of identical SSMs, the other being the mirror image of the first pair. As shown in Fig. 5, the two pairs are arranged in such a way that two output links of the two opposite mechanisms are connected to the correspondent output links of their mirror-image mechanisms, with "S" indicating the SSM connected to the cams, while "I" stands for the mirror-image mechanism. The input shafts of two opposite mechanisms rotate with the same angular velocity, those of their mirror images rotating in the opposite directions but with angular velocities of identical absolute values. Both rotations of the input shafts are transmitted equally to the output shafts. In order to have a symmetric layout, the input shaft of each of the two pairs of mechanisms makes an angle of 135 deg with each of their output shafts, which implies $\alpha_1 = \alpha_7 = 3\pi/4$.

The degree of freedom (dof) of the chain of Stephenson mechanisms warrants discussion. We start by recalling that each SSM has a dof=1. Hence, the coupling of any "S" mechanism with one of its "I" counterparts, to form an open chain of two SSMs, also has a dof=1. Now, if we cut the lower-right shaft of Fig. 5, the chain of Stephenson mechanisms is open, but still composed of four such mechanisms. Let us drive the single-dof open chain with an angular velocity $\dot{\psi}$ of the cut shaft, as input to the lower "I" mechanism. By symmetry, the output angular velocity of the cut shaft, regarded as an output of the right-hand "S" mechanism, is identical to $\dot{\psi}$. We can hence rigidly couple the two parts of the cut shaft, thereby obtaining a single-dof closed chain of SSMs.

**4.2 Computation of the Link Dimensions.** A SSM is now synthesized as outlined in Sec. 3. To define the IO triad, we first produce a four-bar spherical linkage. For the design of this linkage, we draw from the work reported in [30]: upon imposing the conditions for full rotation of the input and the output links, we maximize the transmission quality [31]. A simple case of such a mechanism is the universal joint. Therefore, the parameters of this four-bar spherical linkage can be selected as $\alpha_2 = \alpha_3 = \alpha_4 = \pi/2$.

From an entire motion cycle ($0 \leqslant \psi \leqslant 2\pi$) of the four-bar spherical mechanism, the set $\{\Delta\psi_i, \Delta\gamma_i\}_{i=1}^m$ is obtained. We assume, moreover, that $\Delta\phi_i = \Delta\gamma_i$ in order to obtain a whole set of increments $\{\Delta\psi_i, \Delta\gamma_i, \Delta\phi_i\}_{i=1}^m$. We thus construct the $m$-dimensional vector $\mathbf{q}$ with $m=360$. Moreover, we add one extra equation to the foregoing list of $m=360$ input-output equations, so that $\alpha_3'$ is led to lie close to 90 deg, as explained presently. Recalling

$$\cos\alpha_3' = \frac{1 - x_8^2}{1 + x_8^2} \quad x_8 = \tan\left(\frac{\alpha_3'}{2}\right)$$

we aim at satisfying the equation

$$1 - x_8^2 = 0 \tag{34}$$

in the least-square sense, which is done by adding one component to vector $\mathbf{q}$, thereby increasing its dimension to 361. Thus,

$$q_{361} = 1 - x_8^2 \tag{35}$$

Hence, we end up with a weighted, nonlinear least-square problem of the form of Eq. (32), with weighting matrix $\mathbf{W}$ defined as

$$\mathbf{W} = \mathrm{diag}(w_1, w_2, \ldots, w_{360}, w_{361}) \tag{36}$$

The problem was solved using the Optimization Toolbox of MATLAB V6.5 with the LSQNONLIN function, which yielded the link dimensions listed in row A of Table 1. These results were obtained with the weights below:

$$w_1 = w_2 = \cdots = w_{360} = \frac{0.9}{360} \quad w_{361} = 0.1$$

which are normalized so that they add up to unity, the weighted rms value of the error being

$$e = 1.32 \times 10^{-5} \text{ rad}$$

which is quite acceptable.

**4.3 Mechanism Design.** The dimensions of the spherical Stephenson mechanism obtained in Sec. 4.2 are adjusted by rounding them off to the closest integer multiple of 5.0 deg, thereby obtaining the dimensions listed in row B of Table 1. It is noteworthy that such a dimension adjustment is bound to affect the motion of the mechanism. In our design, the difference between the output angular displacements of the synthesized and the adjusted SSM is shown in Fig. 6, which indicates maximum differences of 1.5 deg for $\psi$ and 5.0 deg for $\gamma$. It is noted that the effect of such differences on the mechanism operation is null, since we are interested only in finding a mechanism with a crank

**Table 1 Link dimensions of a SSM**

| | $\alpha_1$ | $\alpha_2$ | $\alpha_3$ | $\alpha_3'$ | $\alpha_4$ | $\alpha_5$ | $\alpha_6$ | $\alpha_7$ | $\beta$ |
|---|---|---|---|---|---|---|---|---|---|
| A | 135° | 84.75° | 70.25° | 88.99° | 86.08° | 76.99° | 83.23° | 135° | 56.85° |
| B | 135° | 85° | 70° | 90° | 85° | 75° | 85° | 135° | 55° |

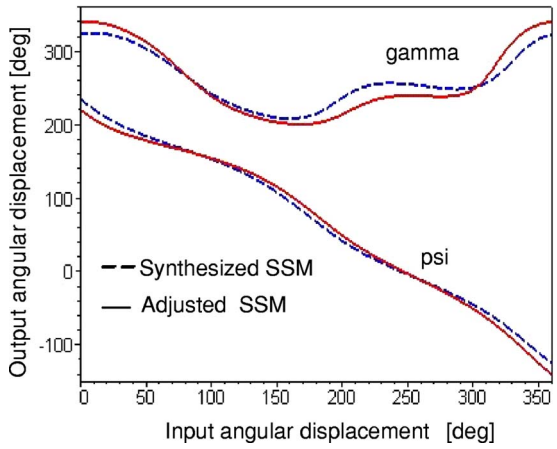


**Fig. 6 Angular displacements of the SSM**

output. Moreover, the two transmission angles, $\mu$ of the four-bar loop and $\nu$ of the five-bar loop, as plotted in Fig. 7, lie within the range [20 deg, 144 deg]. This implies a deadlock-free transmission.

A practical problem in designing the mechanism is the interference among moving links, which is common for multibar planar and spatial mechanisms. For planar mechanisms, interference can be avoided by laying out the links in different planes or by positioning input and output shafts so as to free space for the moving links. A similar strategy can also be applied to some single-input/single-output spherical mechanisms. However, interference in a SSM cannot be eliminated simply by resorting to the foregoing solution, since interference occurs not only among links, but also among links and input or output shafts. The multiclosed loop nature of the SSM makes any moving link prone to collisions with one of the three shafts. To solve this problem, we streamlined the embodiment. In particular, we shaped the coupler link to accommodate the motion of the other links. Considering that all joints intersect at the sphere center, the coupler shape, schematically a spherical triangle as displayed in Fig. 8(*a*), was streamlined as a combination of three bars, as depicted in Fig. 8(*b*). The same link is finally given the embodiment shown in Fig. 8(*c*), using the cross element of an off-the-shelf universal joint, namely, the 302-0400 cross and bearing of G & G Manufacturing Co., with a link added at its end. Such a design can effectively reduce the elastic deformation of the coupler link. The right angle of the coupler

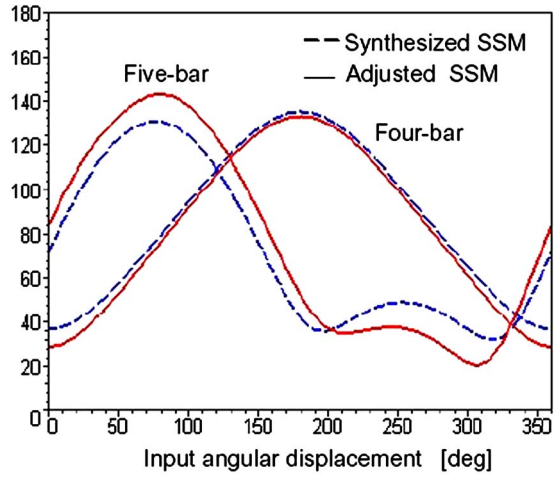


**Fig. 7 Transmission angles of the four- and five-bar loops**

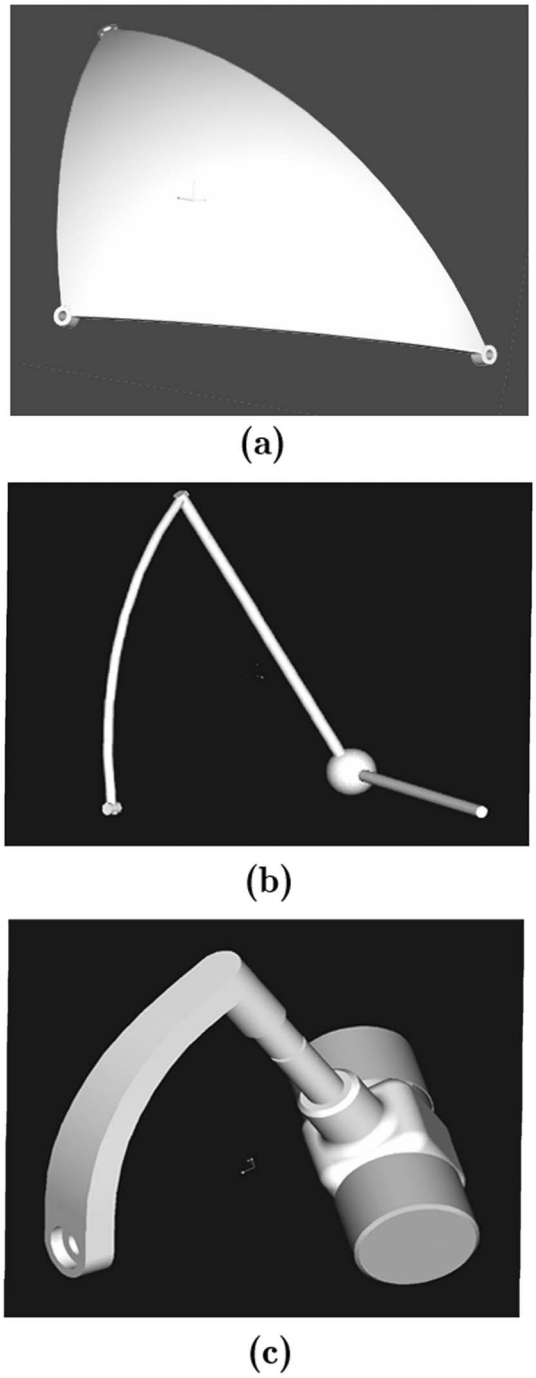


**Fig. 8 The embodiment of the coupler link: (*a*) spherical triangle; (*b*) streamlined embodiment; (*c*) coupler designed based on the cross element of an off-the-shelf universal joint with an added link at its end**

means $\alpha_3'=90$ deg, as per Eq. (34). Accommodating to the shape of the coupler, the input shaft has a yoke shape at one of its end, as illustrated in Fig. 9(*a*).

The chain of SSMs is designed as shown in Fig. 9(*b*), which shows the array of two SSMs and their mirror images. The whole chain is mounted on a cam-carrier, which plays the role of the planet carrier of conventional differential trains of bevel gears. The pitch-roll wrist consisting of the SSM chains and spherical cams is displayed in Fig. 9(*c*).

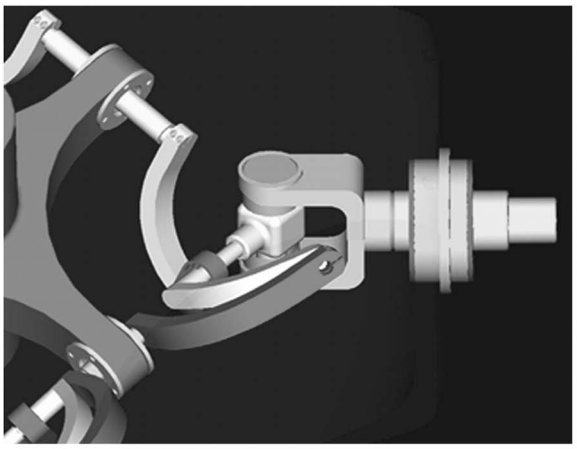

(a)

(b)

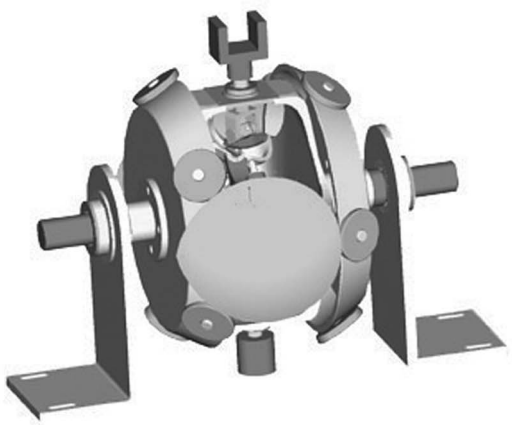

(c)

**Fig. 9 A rotation-reversal mechanism based on SSMs: (*a*) single SSM; (*b*) array of two SSMs and their mirror images; (*c*) view of the pitch-roll wrist designed with the rotation-reversal mechanism**

## 5 Conclusions

A gearless pitch-roll wrist consisting of cam-rollers and spherical Stephenson mechanisms (SSMs) was introduced here. The design of the SSMs is described with emphasis on the dimensional synthesis. The problem of interference-avoidance is solved by proper embodiment of all the links.

Given the shape of the coupler, its dynamic properties may become undesirable due to its nonsymmetric geometry. Therefore, a shape optimization is required for the coupler to enhance the dynamic performance of the SSM. The dynamic balancing through shape optimization of all the links is in our plans.

## Acknowledgment

The research work reported here was made possible by Grant No. 246488-01 of Canada's Natural Sciences and Engineering Research Council. The support of our two industrial partners, Alta Precision Inc. Montreal, and Placage Unique Inc,. Rigaud (QC), Canada, is dutifully acknowledged.

## References

[1] Howard, R. D., 2002, "Design of a Robotic Wrist and Tool-Exchange Mechanism for Satellite Servicing," Proc. 36th Aerospace Mechanism Symposium, NASA Glenn Research Center. The PDF file of this reference was downloaded from: http://www.ssl.umd.edu/publications/. Unfortunately, this file does not include place and page numbers.

[2] Yang, D. C. H., Lin, E. Y., and Cheng, S. Y., 1990, "Primary Workspace of Industrial Robots With Roll-Pitch-Yaw Wrists," ASME J. Mech. Des., **112**(3), pp. 347–353.

[3] Rauchfuss, J. W., and Yang, D. C. H., 2000, "A Geometric Approach for Determining Exact Point Accessibility of Robotic Manipulations," ASME J. Mech. Des., **122**(3), pp. 287–293.

[4] Tsai, L.-W., 1988, "The Kinematics of Spatial Robotic Bevel-Gear Trains," IEEE J. Rob. Autom., **4**(2), pp. 150–156.

[5] Yang, D., and Rauchfuss, J., 2001, "A New Zero-Dimension Robot Wrist: Design and Accessibility Analysis," Int. J. Robot. Res., **20**(2), pp. 163–173.

[6] Gosselin, C. J., and Cloutier, L., 1993, "The Generating Space for Parabolic Motion Error Spiral Bevel Gears Cut by Gleason Method," ASME J. Mech. Des., **115**(3), pp. 483–489.

[7] Wiitala, J. M., and Stanisic, M. M., 2000, "Design of an Overconstrained and Dextrous Spherical Wrist," ASME J. Mech. Des., **122**(3), pp. 347–353.

[8] Bidault, F., Teng, C. P., and Angeles, J., 2001, "Structural Optimization of a Spherical Parallel Manipulator Using a Two-Level Approach," *Proc. of ASME 2001 Design Engineering Technical Conferences*, DAC-21030.

[9] Gosselin, C., and Hamel, J.-F., 1994, "The Agile Eye: A High-Performance Three-Degree-of-Freedom Camera-Orienting Device," *Proc. IEEE Int. Conf. on Robotics and Automation*, pp. 781–786.

[10] Ghuneim, T., Angeles, J., and Bai, S., 2004, "The Design of a Novel Pitch-Roll Wrist With Spherical Cam-Roller Pairs," in *On Advances in Robot Kinematics* J. Lenarcic and C. Galletti, eds., Kluwer Academic Publishers, Dordrecht, pp. 381–388.

[11] Gonzlez-Palacios, M., and Angeles, J., 1999, "The Design of a Novel Mechanical Transmission for Speed Reduction," ASME J. Mech. Des., **121**(4), pp. 538–543.

[12] Gonzlez-Palacios, M., and Angeles, J., 2003, "The Design of a Novel Pure-Rolling Transmission to Convert Rotational into Translational Motion," ASME J. Mech. Des., **125**(1), pp. 205–207.

[13] Primrose, E., Freudenstein, F., and Roth, B., 1967, "Six-Bar Motion. II. The Stepenson-1 and Stephenson-2 Mechanism," Arch. Ration. Mech. Anal., **24**, pp. 42–72.

[14] Suh, C. H., and Mecklenburg, A. W., 1973, "Optimal Design of Mechanisms With the use of Matrices and Least Squares," Mech. Mach. Theory, **8**(4), pp. 479–495.

[15] McLarnan, C., 1963, "Synthesis of Six-Link Plane Mechanisms by Numerical Analysis," ASME J. Eng. Ind., **85**(1), pp. 5–11.

[16] Zanganeh, K. E., and Angeles, J., 1993, "A Symbolic Approach to the Input-Output Analysis of the Stephenson Six-Bar Linkage," *Proc. 1993 ASME Design Engineering Technical Conferences*, Albuquerque, Sept. 19–22, Vol. 2, pp. 67–72.

[17] Baker, J. E., 2004, "The Closure Modes of Bennett's Twelve-Bar Planar Linkage," ASME J. Mech. Des., **126**(3), pp. 464–469.

[18] Dhingra, A., Cheng, J., and Kohli, D., 1996, "Synthesis of Six-Link, Slider-Crank and Four-Link Mechanisms for Function, Path and Motion Generation Using Homotopy With *m*-Homogenization," ASME J. Mech. Des., **116**(4), pp. 1122–1131.

[19] Schreiber, H., Meer, K., and Schmitt, B. J., 2002, "Dimensional Synthesis of Planar Stephenson Mechanisms for Motion Generation Using Circlepoint Search and Homotopy Methods," Mech. Mach. Theory, **37**(7), pp. 717–737.

[20] Sakamoto, Y., Ogawa, K., and Funabashi, H., 1994, "A Kinematic Analysis of Planar Six-Bar Mechansims With Consideration of the Interference of Moving Links," Mech. Mach. Theory, **29**(3), pp. 345–356.

[21] Chiang, C., 1988, *Kinematics of Spherical Mechanism*, Cambridge University Press, Cambridge.

[22] Kohli, D., and Khonji, A., 1994, "Grashof-type of Rotatability Criteria of Spherical Five-Bar Linkages," ASME J. Mech. Des., **118**(3), pp. 99–104.

[23] Farhang, K., and Zargar, Y., 1999, "Design of Spherical 4R Mechanisms: Function Generation for the Entire Motion Cycle," ASME J. Mech. Des., **121**(12), pp. 521–528.
[24] Ge, Q. J., and McCarthy, J. M., 1991, "The Algebraic Classification of the Image Curves of Spherical Four-Bar Motion," ASME J. Mech. Des., **113**(3), pp. 227–231.
[25] Ge, Q. J., and Larochelle, P. M., 1999, "Algebraic Motion Approximation With NURBS Motions and its Application to Spherical Mechanism Synthesis," ASME J. Mech. Des., **121**(12), pp. 529–532.
[26] Larochelle, P. M., and McCarthy, J., 1994, "Design of Spatial 4C Mechanisms for Rigid-Body Guidance," *Proc. 23rd Biennial Mechanisms Conference*, Minneapolis, Sept. 11–14, Vol. 70, pp. 135–142.
[27] Wampler, C. W., 2004, "Displacement Analysis of Spherical Mechanisms Having Three or Fewer Loops," ASME J. Mech. Des., **126**(1), pp. 93–100.
[28] Salmon, G., 1885, *Lessons Introductory to the Modern Higher Algebra*, Chelsea Publishing Co., New York.
[29] Angeles, J., and Zakhariev, E., 1998, *Computational Methods in Mechanical Systems*, Springer-Verlag, Heidelberg.
[30] Zanganeh, K. E., and Angeles, J., 1994, "On the Optimum Design of Planar and Spherical Drag-Link Mechanisms," ASME Journal of Mechanism Syntheis and Analysis, **70**(4), pp. 183–190.
[31] Gosselin, C., and Angeles, J., 1989, "Optimization of Planar and Spherical Function Generators as Minimum-Defect Linkages," Mech. Mach. Theory, **24**(4), pp. 293–307.